PHYSICAL REVIEW B **108**, 035145 (2023)

Magnetic proximity effects at a ferrite–5*d*-metal interface: GGA+U calculations

K. Knížek[*] and Z. Jirák
Institute of Physics of the CAS, Cukrovarnická 10, 162 00 Prague 6, Czech Republic

(Received 28 March 2023; revised 17 June 2023; accepted 13 July 2023; published 24 July 2023)

We have studied spin polarization due to proximity effect at the interface of nonmagnetic 5d metal (Me = Ta, W, Re, Os, Ir, Pt, and Au) and ferrimagnetic conducting (mixed-valence) magnetite Fe_3O_4 or insulating maghemite γ-Fe_2O_3 using *ab initio* electronic structure calculations. Four variants of chemical bonding at the interfaces have been modeled. It appears that the moments induced are oriented according to spin orientation of Fe ions to which Me atoms are bonded-parallel for the direct Fe-Me exchange path and antiparallel for the Fe-O-Me superexchange. The obtained densities of states show that notable spin polarization occurs only for Me atomic plane at very vicinity of the interface with the ferrite. The effect is maximum ~0.2–0.3 μ_B for Pt, where slightly higher moment is induced by insulating γ-Fe_2O_3. Among other metals the moment of ~0.1 μ_B is calculated for Ir. The moment induced in Ta is also relatively large ~0.1 μ_B, but with opposite sign and only in the case of Fe-Me bonding. The exceptional behavior of Pt can be associated with the position of its Fermi level (E_F) near the edge of the wide 5d band at a local peak of density of states (spin-nonpolarized DOS = 6.2 eV^{-1} *per* atom).

DOI: 10.1103/PhysRevB.108.035145

I. INTRODUCTION

The spin Seebeck effect (SSE) discovered in 2008 by Uchida *et al.* [1–4] is one of the principal elements of the emerged field of spintronics. In SSE, the temperature gradient imposed to magnetically ordered material, typically ferro- or ferrimagnet (FM), generates a spin voltage in the same direction. This enables injection of spin currents into an attached nonmagnetic metal (Me), where the spin currents produce a transverse charge voltage by means of the inverse spin Hall effect (ISHE) with spin Hall angle as a characteristic parameter [5]. An analogous effect measured using the same geometry is the anomalous Nernst effect (ANE). The difference is that in case of ANE the charge voltage is generated directly in the magnetic material without any additional layer. In analogy to the classical Seebeck effect, the coefficients of SSE+ISHE and ANE are defined as a ratio of the generated electric field and applied thermal gradient $E/\triangle T$.

In the analysis of SSE, additional factors influencing the spin injection must be taken into account. These are namely, the spin mixing conductance that determines the spin transmission and spin backflow of the FM/Me interface [6], and the coupling between the magnetization in FM and the ordered spins in Me due to the magnetic proximity effects (MPE). The role of these effects has been demonstrated in particular for platinum which possesses a large positive spin Hall angle and is among the most efficient representatives for spin current detection using ISHE. The SSE measurement might be contaminated by ANE generated in the magnetized part of the Pt layer [7,8]. Such an interface-induced ANE was observed in Pt/Fe_3O_4 by using modified configuration with transverse orientation of external field, for which SSE was absent and only the ANE from the ferromagnetic layers or magnetic proximity effects could be detected. The thermoelectric voltage produced by ANE was found small, suggesting that the spin Seebeck effect is the dominant mechanism for the signal measured at standard experimental configuration [9].

The direct determination of MPE at the interface with FM was investigated by x-ray circular magnetic dichroism (XMCD) measurements at the Pt L_3 edge and by x-ray resonant magnetic reflectivity (XRMR). Strong spin polarization was found in Pt films patterned onto elemental 3d ferromagnets. In a detailed analysis of Pt/Co data it was shown that Pt atom has a magnetic moment of 0.61 μ_B at the interface, and the moment decreases exponentially with the distance from the interface with a characteristic decay length of 0.41 nm. Four atomic Pt layers near the interface thus possess 90% of the total magnetization of Pt [10]. A similarly clear XMCD signal was identified for Pt/Fe bilayers, and magnetic moment per spin polarized Pt atom at the interface was determined by XRMR to be up to 0.6 μ_B [11,12].

No XMCD signal as the signature of an induced magnetism in Pt was detected for a series of insulating and conducting ferrites at the Pt/MFe_2O_4 interface (M = Mn, Co, Ni and Fe) [12–14]. On the other hand, XMCD measurements in a Fe_3O_4/Pt/Fe_3O_4 trilayer grown at high temperature showed a large induced magnetic moment in the Pt interlayer [15]. Similar controversy exists for Pt layers on intrinsic magnetic insulator $Y_3Fe_5O_{12}$. For Pt/$Y_3Fe_5O_{12}$ bilayers with Pt thickness of 3 nm (~13 atomic layers), no or only negligible moments of 0.003 μ_B per Pt atom could be deduced from measured XMCD signal [11]. In contrast, a notably larger induced moment of 0.054 μ_B on average was found for a bilayer with Pt thickness of 1.5 nm in a study of another group [16]. Also the strong ferromagnetic characteristics found in

---

[*] Corresponding author: knizek@fzu.cz

2469-9950/2023/108(3)/035145(8)

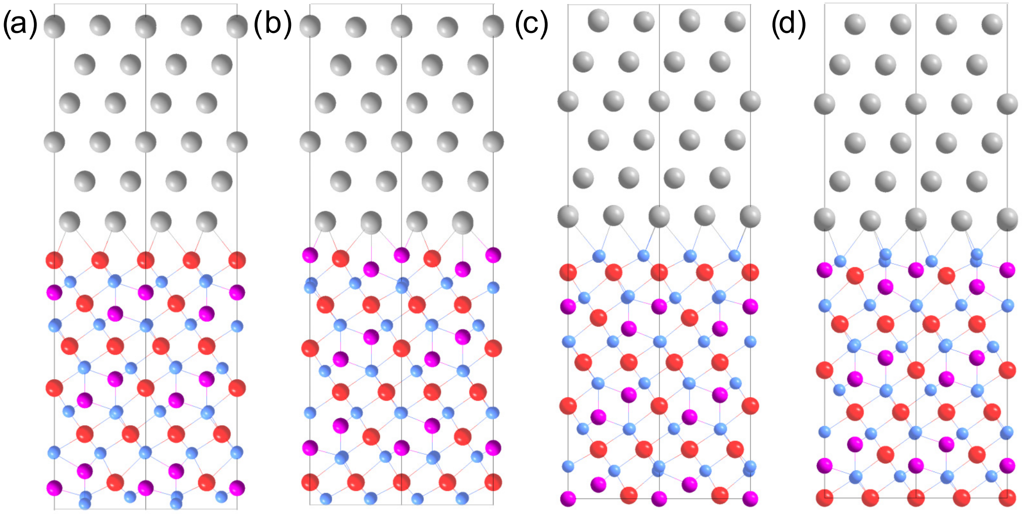

FIG. 1. The hexagonal superlattice of Me/Fe_3O_4 (supercell $Fe_{18}O_{24}Me_{24}$) showing four possible types of interfaces (a) Fe(octahedra)-Me, (b) Fe(tetrahedra)-Me, (c) Fe(octahedra)-O-Me, (d) Fe(tetrahedra)-O-Me. Lattice parameter $a_{\mathrm{hex}} = a_{\mathrm{cub}}/\sqrt{2} = 5.936$ Å was fixed at average experimental value for all Me/Fe_3O_4 and Me/γ-Fe_2O_3. Parameters c were optimized for each Me/Fe_3O_4: $c = 29.951$ Å (Ta), $c = 29.105$ Å (W), $c = 28.840$ Å (Re), $c = 28.810$ Å (Os), $c = 28.840$ Å (Ir), $c = 28.999$ Å (Pt), $c = 29.793$ Å (Au). The structures of Me/γ-Fe_2O_3 were created by removing two Fe(octahedra) atoms from the middle layers (supercell $Fe_{16}O_{24}Me_{24}$), the optimized parameters c are: $c = 29.158$ Å (Ta), $c = 28.311$ Å (W), $c = 28.046$ Å (Re), $c = 28.005$ Å (Os), $c = 28.046$ Å (Ir), $c = 28.205$ Å (Pt), $c = 28.999$ Å (Au). The atoms in the structure are displayed as (●) Me, (●) Fe(octahedra), (●) Fe(tetrahedra), (●) O.

electrical and thermal magnetotransport measurements on thin Pt films patterned on $Y_3Fe_5O_{12}$ confirmed a presence of magnetic proximity effect [7].

Gold represents a 5d metal with a significantly smaller spin Hall angle compared to Pt [17–19]. The calculations based on spin polarized density functional theory (DFT) did not show any induced moment of Au layers at the proximity of the interface with $Y_3Fe_5O_{12}$. The same model applied to Pt layers confirmed significant spin polarization of Pt atoms and their ferromagnetic coupling to neighboring Fe atoms in $Y_3Fe_5O_{12}$ [8,20]. Another notable representative is Ta, which can be characterized as a counterpart of Pt, as it also exhibits a remarkable spin Hall angle, but with the opposite sign [18,21,22]. Among 3d-metals, large spin Hall angle but negligible magnetic proximity effect was observed for Cr [23]. Since the presence of MPE entails other disturbing effects, such as magnetoresistance or the anomalous Hall effect, for a fundamental investigation of spin current phenomena, it is useful to verify whether the metal used is a pure detector of spin current without MPE. In addition, in this paper we want to point out that the magnetic proximity effect may depend not only on the metal, but also on the properties of the ferromagnetic material, in particular the type of magnetic arrangement, its insulator/conductor character or bonding type at the interface (cation-Me/cation-O-Me).

In order to compare the importance of MPE in Pt and other transition metals, which might be used for the spin current detection, we have performed a generalized gradient approximation (GGA)+U calculation of MPE for a series of 5d transition metals Me = Ta, W, Re, Os, Ir, Pt, and Au, interfaced with FM material. For the latter we selected magnetite Fe_3O_4 based on the following reasons: (1) Both Fe-metal and Fe-oxygen-metal interfaces can be studied. (2) A relatively simple crystal structure is found of the spinel type and a magnetic structure with ferrimagnetic ordering is also found. (3) The conducting Fe_3O_4 can be easily converted to insulating γ-Fe_2O_3 (maghemite) by creating a small number of vacancies on Fe sites, thus allowing investigation of MPE induced by both conducting and insulating FM. (4) The spin Seebeck effect and anomalous Nernst effect were thoroughly experimentally studied in Pt/Fe_3O_4 [24–30] and also in Pt/γ-Fe_2O_3 [31].

II. METHOD OF CALCULATION

We applied the model of the Me/Fe_3O_4 and Me/γ-Fe_2O_3 hexagonal superlattice consisting of an alternation of ferrite layers of ∼1.5 nm thickness and Me layers of similar thickness, see Fig. 1. The supercell $Fe_{18}O_{24}Me_{24}$ was used for Me/Fe_3O_4 and $Fe_{16}O_{24}Me_{24}$ for Me/γ-Fe_2O_3. More details about the construction of the superlattices can be found in the Supplemental Material [32]. The lattice mismatch calculated between the a parameter of hexagonal cell constructed from the Fe_3O_4 cubic cell and a parameters of hexagonal cells of individual transition metals Me constructed using the appropriate matrices is shown in Table S1 in the Supplemental Material [32]. The lattice parameters of Me hexagonal cells are generally smaller and the mismatch ranges between 0 and 10%. Comparison of Me-Me interatomic distances obtained experimentally and obtained from the relaxed supercell is also shown. It can be seen that the relaxation of the c parameter partially reduces the mismatch of the experimental and relaxed Me-Me distances, which ranges between 2 and 7%.

The structures of the supercells for each Me/FeO_x combinations were relaxed with respect to minimal calculated forces on all atoms during the electronic structure calculations. The calculations were made with the WIEN2k program [33]. This program is based on the DFT and uses the full-potential linearized augmented plane-wave (FP LAPW) method with the dual basis set. In the LAPW methods, the space is divided into atomic spheres and the interstitial region. The electron states are then classified as the core states fully contained in the atomic spheres, and the valence states. The core states were defined as an electronic configuration (Ne $3s^2$) for Fe, as (He) for O and as (Kr $4d^{10}$) for $5d$ metals. The radii of the atomic spheres were taken at 1.95 a.u. for Fe, 1.52 a.u. for O and 2.3 a.u. for $5d$ metals. The number of k points in the irreducible part of the Brillouin zone was 8, which is sufficient for the big unit cell used. For the exchange correlation potential we adopted the GGA form [34]. The initial orientations of the magnetic moments on the Fe atoms were set according to the known ferrimagnetic structure. The metal atoms were not spin polarized at the beginning of the calculation.

To improve the description of $3d$ electrons in Fe we used the GGA+U method. In this method, an orbitally dependent potential is introduced for the chosen set of electron states, i.e., for $3d$ states in our case. This additional potential has an atomic Hartree-Fock form but with screened Coulomb and exchange interaction parameters. The fully localized limit version of the GGA+U method was employed, using Hubbard U correction for Fe-$3d$ orbitals. The parameters $U = 6.8$ eV and $J = 0.95$ eV were used, which are typical values used in Fe_3O_4 or $BaFe_{12}O_{19}$ [35,36].

The atomic charges and magnetic moments were calculated using the atoms in molecule (AIM) concept of Bader [37]. In this approach, the charge or magnetic moment at a given site is calculated by integrating the electron/spin density inside regions delimited by minima in the respective density. The advantage of this method is that the analysis is independent of the basis set and atomic spheres used. Let us note that the AIM method takes into account the charge transfer between cation and ligands, therefore the calculated charges are lower than the ideal ones, depending on the degree of covalency.

III. RESULTS AND DISCUSSION

Fe_3O_4 crystalizes in cubic spinel structure of the space group symmetry $Fd\bar{3}m$ with typical lattice parameter $a =$ 8.395 Å. Oxygen atoms form a face-centered-cubic network, in which iron atoms occupy 1/8 of interstices with tetrahedral coordination (A sites), and 1/2 of interstices with octahedral coordination (B sites). The magnetic arrangement is ferrimagnetic with majority spins on octahedral sites and minority spins with opposite orientation on tetrahedral sites. The ideal valence of Fe on tetrahedral sites is 3+ and on octahedral sites is mixed 2+/3+. Due to this mixed valency the density of states (DOS) at Fermi level is nonzero [38], and the phase display a poor metallic conductivity above the temperature ~120 K (Note that below 120 K the Verwey transition takes place, leading to a charge ordering of the Fe^{2+} and Fe^{3+} states on B sublattice [39]). The magnetic moments determined experimentally at low temperature are $m_A = -4.44\ \mu_B$ (A site) and $m_B = 4.17\ \mu_B$ (B site), which results in saturated ferrimagnetic moment $m = 2m_B + m_A = 3.9\ \mu_B/f.u.$ (*f.u.* = formula unit of Fe_3O_4) [39]. Similar values were calculated by the AIM method [37] using the electron density obtained by the GGA+U method, namely $m_A = -4.46\ \mu_B$, $m_B = 4.27\ \mu_B$ and $m_O = -0.02\ \mu_B$, which gives in total $m = 4.0\ \mu_B/f.u.$ [38].

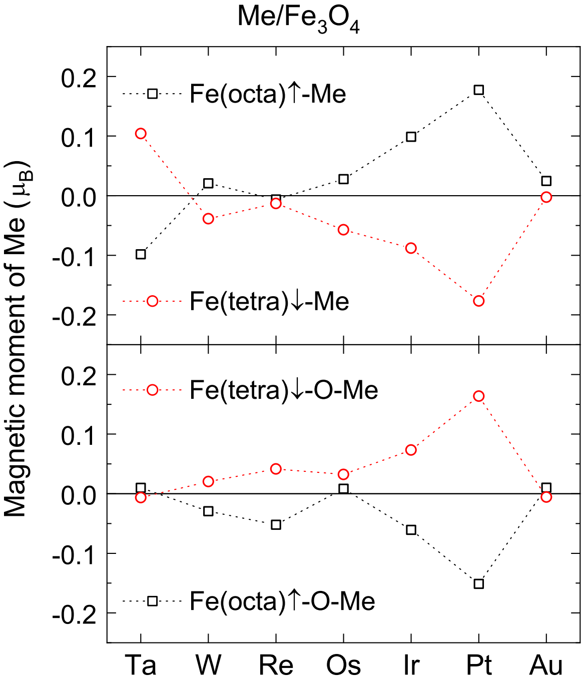

FIG. 2. Comparison of the induced magnetic moment for various $5d$ transition metals Me = Ta, W, Re, Os, Ir, Pt and Au in the composites with conducting Me/Fe_3O_4 for various Fe coordinations (octahedra/tetrahedra) and Fe-Me/Fe-O-Me bonding.

Maghemite γ-Fe_2O_3 crystalizes in the same spinel structure, the difference consists of iron vacancies occurring in 1/6 of the B sites. The important consequence is that now there is no longer mixed valency in the B site, so the Fe valency is 3+ in both A and B sites and a gap in DOS around 2 eV opens [40].

Two crystallographic sites of Fe with different coordinations and opposite spin orientation, and possibility of either direct bonding between Fe and Me or bonding via oxygen, creates four possible variants of interfaces between Fe and metal (Me) at the atomic level in Fe_3O_4. These are namely, (1) Fe(octahedral, spin up)-Me, (2) Fe(tetrahedral, spin down)-Me, (3) Fe(octahedral, spin up)-O-Me, and (4) Fe(tetrahedral, spin down)-O-Me. The same four variants were tested for γ-Fe_2O_3. The calculated magnetic moments induced in the Me atoms lying in the plane nearest to the FeO_x are displayed in Fig. 2. for Fe_3O_4 and Fig. 3. for γ-Fe_2O_3. The calculations confirm significant magnetic proximity effect in Pt of ~0.2-0.3 μ_B per Pt atom. Sizeable moments of ~0.1 μ_B are also observed for Ir with the same sign as for Pt, and ~0.1 μ_B for Ta with the opposite sign to Pt. Induced moments in the other tested transition metals were generally much smaller. The orientation of the induced spin depends on the orientation of the spin of the interfaced Fe and on the type of the bonding.

For the interface with Fe-metal bonding, the orientation of the induced spin in Pt is parallel to the corresponding Fe site. Thus the up spin on the Fe(octahedra) site induces up spin in the interfaced Pt, whereas down spin on the Fe(tetrahedra) site induces down spin in Pt. The responsible interaction is the

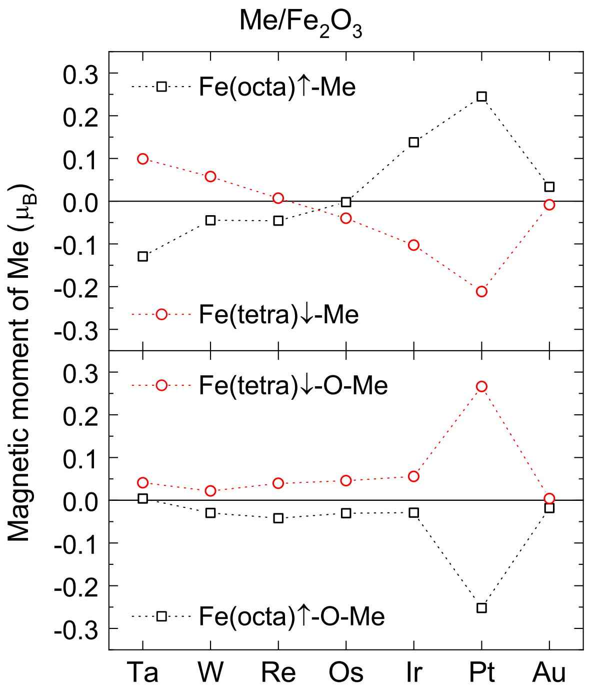

FIG. 3. Comparison of the induced magnetic moment for various $5d$ transition metals Me = Ta, W, Re, Os, Ir, Pt and Au in the composites with insulating Me/γ-Fe$_2$O$_3$ for various Fe coordinations (octahedra/tetrahedra) and Fe-Me/Fe-O-Me bonding.

direct exchange between partially filled *d* orbitals of Fe and Pt. A special case is represented by Ta, for which the exchange coupling has opposite sign.

The DOS of five selected layers of the interface between Fe(octahedra)-Pt is displayed in Fig. 4(a), while complete data for all $5d$ metals are presented in Fig. S2 of the Supplemental Material [32]. The exceptional behavior of Pt can be associated with the position of its Fermi level (E_F) near the edge of the wide $5d$ band where the peak of spin-non-polarized DOS (6.2 eV^{-1} *per* atom) is located. This is a signature of a ferromagnetic instability of Pt. The Fe(octahedra)-*d* spin down band at the E_F is broadened and shifted to lower energies due to the hybridization with Pt-*d* band, compared to narrow band in the Fe$_3$O$_4$ itself, see Fig. S1 of the Supplemental Material [32] adapted from Ref. [38]. The spin up band is also broadened and shifted up close to Fermi level, however, the DOS is still zero at E_F so it remains spin polarized with gap for spin up.

The analogous DOS of the interface between Fe(tetrahedra)-Pt is displayed in Fig. 4(b) and for all Me in Fig. S3 in the Supplemental Material [32]. Although the initial positions of the Fe(tetrahedra)-*d* bands are far below and above the Fermi level in distinction to Fe(octahedra)-*d* bands, see Fig. S1 of the Supplemental Material [32], they are broadened due to the interaction with Pt bands and the spin up gap is closed.

The corresponding changes of electron density are displayed in the simplified scheme at the lower part of Fig. 4. The number of arrows, indicating the electron transfer between atoms and orbitals, roughly corresponds to the amount of electrons transferred. The positive magnetic moment in Pt at the Fe(octahedra)-Pt interface is created due to transfer of electrons realized from the Pt-*d* to the Fe-*d* minority spin orbitals, and in the same amount but opposite direction for majority spin orbitals. Therefore, the spin moment is created in Pt without changing the total number of electrons in this site. Similar electron transfer but in opposite directions, is responsible for creating negative magnetic moment in Pt in the case of Fe(tetrahedra)-Pt interface. The electron transfer from interfaced Fe to Pt is compensated by a transfer of electrons from more distant Fe to the interfaced Fe.

TABLE I. Charges and magnetic moments for Fe(octahedra)-Me and Fe(tetrahedra)-Me interfaces and for the atoms more distant from interface (bulk), in the Pt/Fe$_3$O$_4$ superlattice, and for the phase Fe$_3$O$_4$. Pt interface-1 and 2 denotes Pt from the 1.plane and 2.plane from the interface, respectively. The values were calculated using AIM method [37].

	Fe(octahedra)-Me		Fe(tetrahedra)-Me	
	charge	magnetic moment	charge	magnetic moment
Pt bulk	0.02	0.01	0.02	−0.02
Pt interface-2	0.02	0.08	0.02	−0.07
Pt interface-1	0.02	0.18	0.02	−0.18
Fe interface	1.22	3.99	1.24	−4.09
Fe bulk	1.79	4.43	1.80	−4.44
Fe (Fe$_3$O$_4$) [38]	1.68	4.27	1.77	−4.46

The resulting moments and charges are summarized in Table I. It can be seen, that the charges and magnetic moments of interfaced Fe are significantly reduced compared to the more distant “bulk” Fe, both for Fe(octahedra) and Fe(tetrahedra). Comparison of bulk Fe in our superlattice model and Fe in Fe$_3$O$_4$ shows that the magnetic moment and charge in Fe(octahedra) increased and reached the same (absolute) values as in Fe(tetrahedra) in distinction to the Fe$_3$O$_4$, where Fe(tetrahedra) has higher charge and magnetic moment (in absolute value). It is a consequence of the electron transfer between the bulk Fe-*d* orbitals and the interfaced Fe-*d* orbitals, which are broadened by interaction with the wide Pt-*d* orbitals.

Similar reduction of spin moment and increased total number of electrons for the interfaced Fe is observed for all Fe-Me interfaces, regardless of very different induced moments in interfaced metals. This means that the observed changes in electron density for Fe are a consequence of the broadening and shifting to lower energy of the Fe-*d* band due to the interaction with broad Me-*d* band, but they are not correlated with the possible induced spin in Me.

For the interface with Fe-O-Me bonding, the orientation of the induced spin in Pt is the opposite to the corresponding Fe site, i.e., up spin on for Fe(octahedra) site induces down spin, whereas down spin on Fe(tetrahedra) site induces up spin on neighboring Pt. The responsible interaction is the superexchange between Pt and Fe partially filled *d* orbitals over O *sp* orbitals. No significant magnetic moment is induced for Ta in case of Fe-O-Me type of bonding, in distinction to the case of Fe-Me interface.

The DOS of the selected layers of the interface between Fe(octahedra)-O-Pt is displayed in Fig. 5(a) and for all Me in

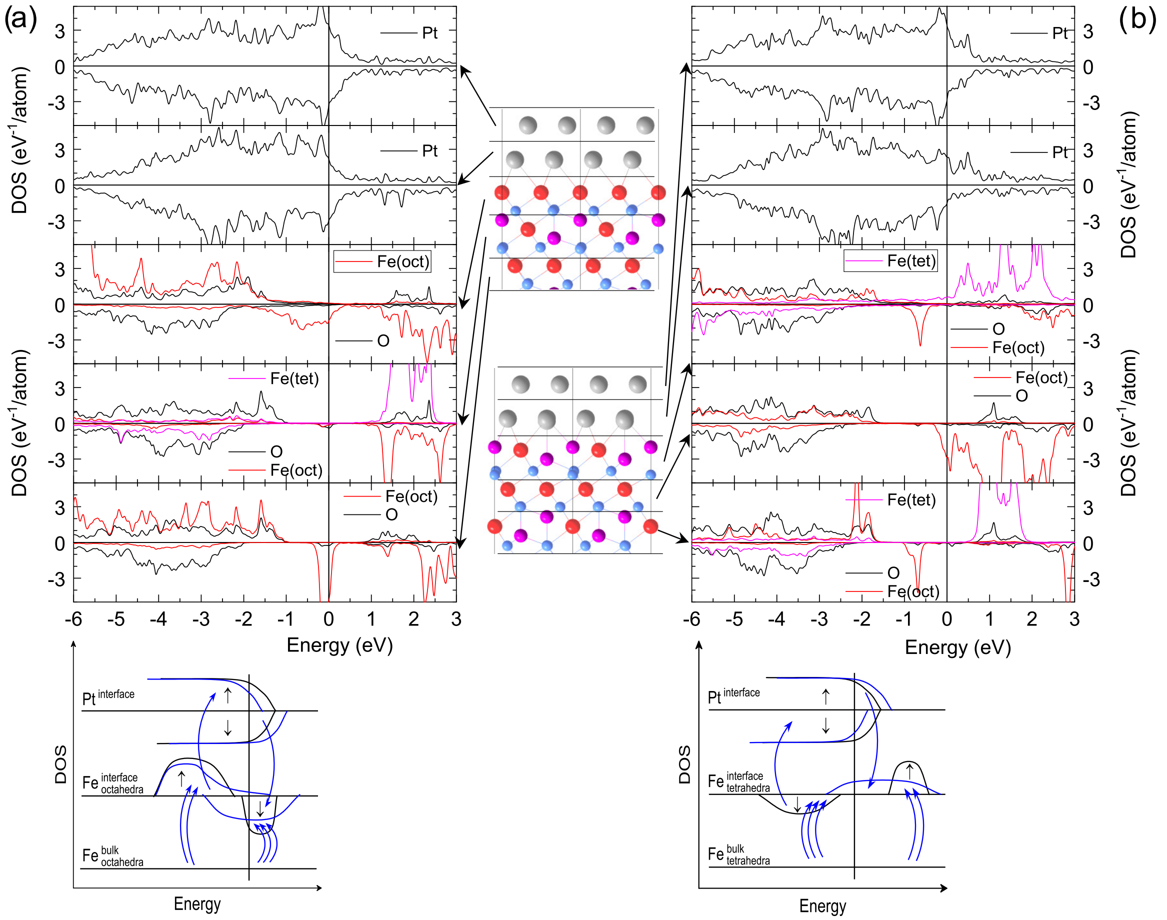

FIG. 4. Density of states of Pt/Fe_3O_4 with interfaces (a) Fe(octahedra)-Pt, (b) Fe(tetrahedra)-Pt. The five panels depicted refer from above, to the second- and first-neighbour Pt atomic layer, followed with the first-, second- and third-neigbour Fe and O layers in the ferrite block. The atoms in the structure are displayed as (●) Pt, (●) Fe(octahedra), (●) Fe(tetrahedra), (●) O. Lower part: scheme of electron transfer between interfaced Fe and Pt, (—) DOS of separated FeO_x and Pt, (—) DOS of Me/FeO_x after electron transfer.

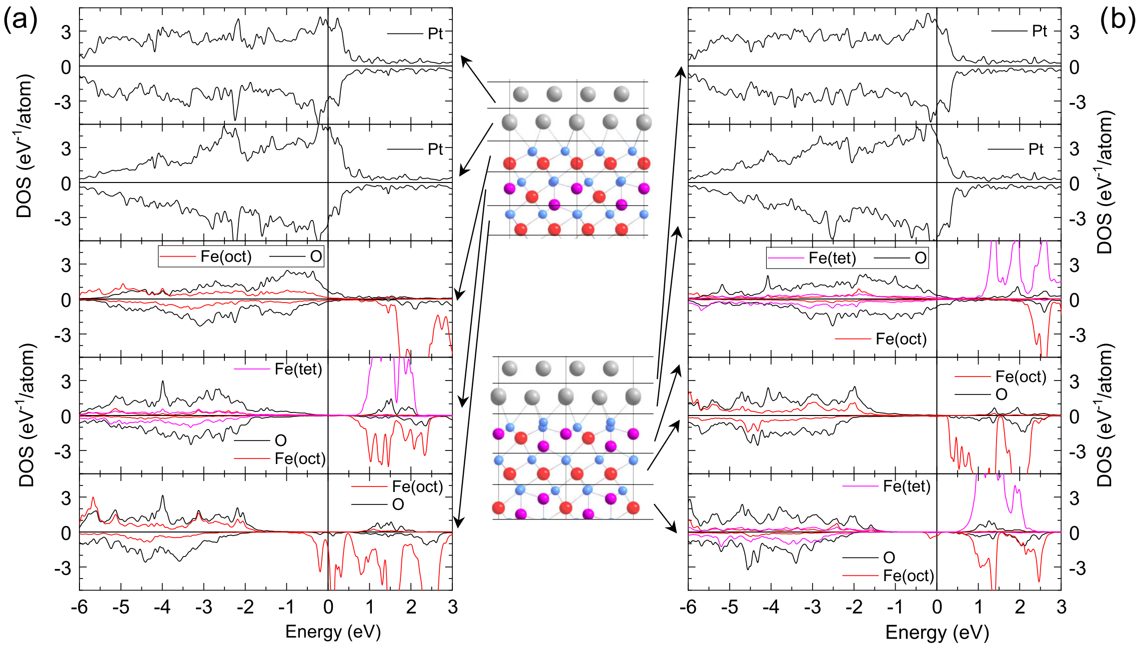

FIG. 5. Density of states of Pt/Fe_3O_4 with interfaces (a) Fe(octahedra)-O-Pt, (b) Fe(tetrahedra)-O-Pt. The five panels depicted refer from above, to the second- and first-neighbour Pt atomic layer, followed with the first-, second- and third-neigbour Fe and O layers in the ferrite block. The atoms in the structure are displayed as (●) Pt, (●) Fe(octahedra), (●) Fe(tetrahedra), (●) O.

Fig. S4 of the Supplemental Material [32]. Significant changes at the DOS around the Fermi level compared to DOS of Fe_3O_4 are again observed. Broad bands with dominant oxygen character are shifted to the Fermi level and partially above for both spin up and spin down, nevertheless the prevailing DOS at E_F is for spin up. The amount of DOS at the Fermi level for interface with other metals is comparable in the case of Ir, for the remaining Me is much lower and for Ta is almost zero. Similar features are observed in the DOS of the interface between Fe(tetrahedra)-O-Pt displayed in Fig. 5(b) and for all Me in Fig. S5 of the Supplemental Material [32], with the exception that in this case the dominant DOS is for spin down. No significant charge transfer is observed in the case of the Fe-O-Me interface, so that the charges of Fe, O, and Me at the interface are equal to the average values of more distant ions.

In addition to four variants of the calculations of MPE in the Me/Fe_3O_4 superlattice, the same calculations have been perfomed for $Me/\gamma\text{-}Fe_2O_3$. The DOS of the selected layers for $Pt/\gamma\text{-}Fe_2O_3$ is presented in Fig. S6 and for $Ta/\gamma\text{-}Fe_2O_3$ in Fig. S7 in the Supplemental Material [32]. It can be seen in Fig. S6 that despite the insulating character of the $\gamma\text{-}Fe_2O_3$, the interfaced Fe in $Pt/\gamma\text{-}Fe_2O_3$ have nonzero DOS at the Fermi level similarly to Pt/Fe_3O_4. We can find that the similarity in the DOS character of the interfaced Fe between Me/Fe_3O_4 and $Me/\gamma\text{-}Fe_2O_3$ is present for all Me. This indicates that the interaction with broad bands of Me is the decisive factor for the resulting character of DOS of the interfaced Fe.

The overall data allow us to compare the influence of various interfaces on the induced magnetic moments in adjacent Me planes and to distinguish what factors are relevant. We have plotted averaged moments for several interfaces in Fig. 6 for illustration. For the sake of comparison, the signs of the induced moments were adapted to Fe(octahedra)-Me interface, so that the moments of Me in Fe(tetrahedra)-Me and Fe(octahedra)-O-Me interfaces were multiplied by −1.

Figure 6(a) manifests the difference between moments induced on Me in conducting Me/Fe_3O_4 and insulating $Me/\gamma\text{-}Fe_2O_3$ by displaying the average over four kinds of Fe(octahedra/tetrahedra)-(O)-Me interfaces. It can be seen that there is no significant difference between them, except for Me = Pt, for which in case of $Me/\gamma\text{-}Fe_2O_3$ the generated moment is about 50% higher.

Figure 6(b) distinguishes between the bonding to Fe(tetrahedral, spin-down) and Fe(octahedral, spin-up) sites, i.e., it averages the moments over Me/FeO_x and Fe-(O)-Me interfaces. This figure reveals that the (absolute) moments induced on Me by interfaced Fe in tetrahedral or octahedral coordinations are practically equal.

Figure 6(c) distinguishes the role of Fe-Me and Fe-O-Me interfaces, i.e., it averages the moments on Me over Me/FeO_x and Fe(octahedra/tetrahedra)-Me interfaces. A notable difference is observed for Ta, for which the moment is only generated at the Fe-Me interface.

In the second Pt plane (Pt interface-2 in Table I), the moment drops to about 1/3 compared to Pt from the first plane at the interface, and it drops to zero in the third plane. This is a sharper decay than reported for Pt films patterned onto ferromagnetic Co and Fe metals, where spin polarization spreads at least up to the fourth Pt plane, decaying in an exponential manner [10]. The explanation may lie in the different nature of the magnetic material. Although we have shown in our work that a ferrimagnetic insulator or a bad conductor produces practically the same MPE, it is still not excluded that the MPE produced by a simple ferromagnetic conductor may have a different character. Another shortcoming may be that the superlattice used in our calculation is not large enough to completely relax the electron density transfers. In our work, we have focused on comparing several different types of interfaces and have shown that in most cases they create the same MPE in respective metals. Therefore, in future work we would like to concentrate on a detailed investigation of selected interface and metals using larger superlattices.

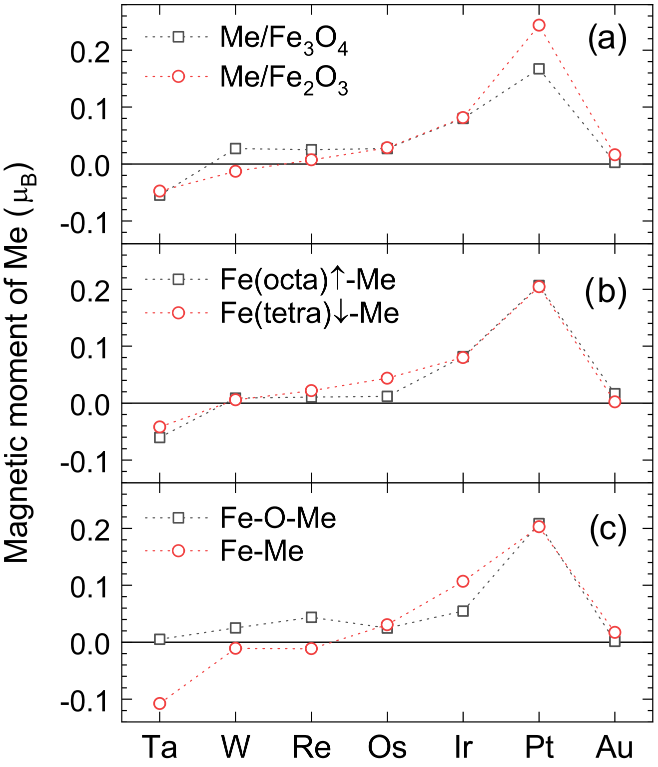

FIG. 6. Comparison of the induced magnetic moment for various 5*d* transition metals Me = Ta, W, Re, Os, Ir, Pt and Au, averaged for several types of interfaces.

IV. CONCLUSIONS

The systems formed by ferro/ferrimagnetic materials interfaced with 5*d* metals have a potential to convert spin currents, created, e.g., by the SSE, into an electromotive force *via* the ISHE. One of its important elements is the partial spin polarization of originally nonmagnetic metal due to MPE, which we focused on in the present study. In particular, the electronic structure calculations based on DFT theory were applied for determination of magnetic moments induced at the interface for case of seven 5*d* metals Me = Ta, W, Re, Os, Ir, Pt, and Au. The calculations were done for a superlattice formed by stacking of the ∼1.5 -nm-thick layers of magnetite Fe_3O_4 or maghemite $\gamma\text{-}Fe_2O_3$ and a layer of metal with similar thickness.

The role of factors that are specific for ferrites and decide on the sign of the interaction has been investigated in detail. It appears that the magnetic moments induced are oriented according to spin orientation of Fe ions to which Me atoms are bonded, i.e., spin up for Fe in octahedral coordination and spin down for Fe in tetrahedral coordination. The resulting moment on Me is parallel for the direct Fe-Me exchange path and antiparallel for the Fe-O-Me superexchange. A special case is represented by Ta for which the exchange coupling has opposite sign for Fe-Me bonding and no significant moment is induced in case of Fe-O-Me interface.

The present work may explain some contradictory experimental observations of MPE if the magnetic material is a ferrimagnetic oxide, like $Y_3Fe_5O_{12}$ or Fe_3O_4, since in this case various types of bonds may be formed at the interface and spin polarization depending on the type of bonding may be partially canceled. On the other hand, if FM is a simple ferromagnetic metal with a single type of bonding, the MPE is consistently confirmed in experiments.

ACKNOWLEDGMENTS

This work was supported by the Project No. 19-06433S of the Czech Science Foundation. Computational resources were provided by the e-INFRA CZ Project ID90254, supported by the Ministry of Education, Youth and Sports of the Czech Republic.

[1] K. Uchida, S. Takahashi, K. Harii, J. Ieda, W. Koshibae, K. Ando, S. Maekawa, and E. Saitoh, Observation of the spin Seebeck effect, Nature (London) **455**, 778 (2008).

[2] K. Uchida, J. Xiao, H. Adachi, J. Ohe, S. Takahashi, J. Ieda, T. Ota, Y. Kajiwara, H. Umezawa, H. Kawai, G. E. W. Bauer, S. Maekawa, and E. Saitoh, Spin Seebeck insulator, Nat. Mater. **9**, 894 (2010).

[3] K. Uchida, H. Adachi, T. Ota, H. Nakayama, S. Maekawa, and E. Saitoh, Observation of longitudinal spin-Seebeck effect in magnetic insulators, Appl. Phys. Lett. **97**, 172505 (2010).

[4] H. Adachi, K. Uchida, E. Saitoh, and S. Maekawa, Theory of the spin Seebeck effect, Rep. Prog. Phys. **76**, 036501 (2013).

[5] E. Saitoh, M. Ueda, H. Miyajima, and G. Tatara, Conversion of spin current into charge current at room temperature: Inverse spin-Hall effect, Appl. Phys. Lett. **88**, 182509 (2006).

[6] C.-F. Pai, Y. Ou, L. H. Vilela-Leão, D. C. Ralph, and R. A. Buhrman, Dependence of the efficiency of spin Hall torque on the transparency of Pt/ferromagnetic layer interfaces, Phys. Rev. B **92**, 064426 (2015).

[7] S. Y. Huang, X. Fan, D. Qu, Y. P. Chen, W. G. Wang, J. Wu, T. Y. Chen, J. Q. Xiao, and C. L. Chien, Transport Magnetic Proximity Effects in Platinum, Phys. Rev. Lett. **109**, 107204 (2012).

[8] D. Qu, S. Y. Huang, J. Hu, R. Q. Wu, and C. L. Chien, Intrinsic Spin Seebeck Effect in Au/YIG, Phys. Rev. Lett. **110**, 067206 (2013).

[9] R. Ramos, T. Kikkawa, A. Anadón, I. Lucas, T. Niizeki, K. Uchida, P. A. Algarabel, L. Morellón, M. H. Aguirre, M. R. Ibarra, and E. Saitoh, Interface-induced anomalous Nernst effect in Fe_3O_4/Pt-based heterostructures, Appl. Phys. Lett. **114**, 113902 (2019).

[10] M. Suzuki, H. Muraoka, Y. Inaba, H. Miyagawa, N. Kawamura, T. Shimatsu, H. Maruyanma, N. Ishimatsu, Y. Isohama, and Y. Sonobe, Depth profile of spin and orbital magnetic moments in a subnanometer Pt film on Co, Phys. Rev. B **72**, 054430 (2005).

[11] S. Geprägs, S. Meyer, S. Altmannshofer, M. Opel, F. Wilhelm, A. Rogalev, R. Gross, and S. T. B. Goennenwein, Investigation of induced Pt magnetic polarization in $Pt/Y_3Fe_5O_{12}$ bilayers, Appl. Phys. Lett. **101**, 262407 (2012).

[12] T. Kuschel, C. Klewe, J. M. Schmalhorst, F. Bertram, O. Kuschel, T. Schemme, J. Wollschläger, S. Francoual, J. Strempfer, A. Gupta, M. Meinert, G. Götz, D. Meier, and G. Reiss, Static Magnetic Proximity Effect in $Pt/NiFe_2O_4$ and Pt/Fe Bilayers Investigated by X-Ray Resonant Magnetic Reflectivity, Phys. Rev. Lett. **115**, 097401 (2015).

[13] M. Collet, R. Mattana, J.-B. Moussy, K. Ollefs, S. Collin, C. Deranlot, A. Anane, V. Cros, F. Petroff, F. Wilhelm, and A. Rogalev, Investigating magnetic proximity effects at ferrite / Pt interfaces, Appl. Phys. Lett. **111**, 202401 (2017).

[14] M. Valvidares, N. Dix, M. Isasa, K. Ollefs, F. Wilhelm, A. Rogalev, F. Sánchez, E. Pellegrin, A. Bedoya-Pinto, P. Gargiani, L. E. Hueso, F. Casanova, and J. Fontcuberta, Absence of magnetic proximity effects in magnetoresistive $Pt/CoFe_2O_4$ hybrid interfaces, Phys. Rev. B, **93**, 214415 (2016).

[15] T. Kikkawa, M. Suzuki, R. Ramos, M. H. Aguirre, J. Okabayashi, K. Uchida, I. Lucas, A. Anadón, D. Kikuchi, P. A. Algarabel, L. Morellón, M. R. Ibarra, and E. Saitoh, Interfacial ferromagnetism and atomic structures in high-temperature grown $Fe_3O_4/Pt/Fe_3O_4$ epitaxial trilayers, J. Appl. Phys. **126**, 143903 (2019).

[16] Y. M. Lu, Y. Choi, C. M. Ortega, X. M. Cheng, J. W. Cai, S. Y. Huang, L. Sun, and C. L. Chien, Pt Magnetic Polarization on $Y_3Fe_5O_{12}$ and Magnetotransport Characteristics, Phys. Rev. Lett. **110**, 147207 (2013).

[17] O. Mosendz, J. E. Pearson, F. Y. Fradin, G. E. W. Bauer, S. D. Bader, and A. Hoffmann, Quantifying Spin Hall Angles from Spin Pumping: Experiments and Theory, Phys. Rev. Lett. **104**, 046601 (2010).

[18] H. L. Wang, C. H. Du, Y. Pu, R. Adur, P. C. Hammel, and F. Y. Yang, Scaling of Spin Hall Angle in 3d, 4d, and 5d Metals from $Y_3Fe_5O_{12}$/Metal Spin Pumping, Phys. Rev. Lett. **112**, 197201 (2014).

[19] M. Isasa, E. Villamor, L. E. Hueso, M. Gradhand, and F. Casanova, Temperature dependence of spin diffusion length and spin Hall angle in Au and Pt, Phys. Rev. B **91**, 024402 (2015).

[20] Y. L. Li, K. L. Yao, Q. H. Lu, Z. L. Liu, D. Xi, X. P. Luo, and Q. Ning, Atomic, electronic, and magnetic structure of the $Au(100)/Fe_3O_4(100)$ interface: Density functional theory study, Phys. Rev. B **75**, 165314 (2007).

[21] C. Hahn, G. de Loubens, O. Klein, M. Viret, V. V. Naletov, and J. Ben Youssef, Comparative measurements of inverse spin Hall effects and magnetoresistance in YIG/Pt and YIG/Ta, Phys. Rev. B **87**, 174417 (2013).

[22] N. Vlietstra, J. Shan, B. J. van Wees, M. Isasa, F. Casanova, and J. Ben Youssef, Simultaneous detection of the spin-Hall magnetoresistance and the spin-Seebeck effect in platinum and tantalum on yttrium iron garnet, Phys. Rev. B **90**, 174436 (2014).

[23] D. Qu, S. Y. Huang, and C. L. Chien, Inverse spin Hall effect in Cr: Independence of antiferromagnetic ordering, Phys. Rev. B **92**, 020418(R) (2015).

[24] R. Ramos, T. Kikkawa, K. Uchida, H. Adachi, I. Lucas, M. H. Aguirre, P. Algarabel, L. Morellón, S. Maekawa, E. Saitoh, and M. R. Ibarra, Observation of the spin Seebeck effect in epitaxial Fe_3O_4 thin films, Appl. Phys. Lett. **102**, 072413 (2013).

[25] R. Ramos, M. H. Aguirre, A. Anadón, J. Blasco, I. Lucas, K. Uchida, P. A. Algarabel, L. Morellón, E. Saitoh, and M. R. Ibarra, Anomalous Nernst effect of Fe_3O_4 single crystal, Phys. Rev. B **90**, 054422 (2014).

[26] R. Ramos, T. Kikkawa, M. H. Aguirre, I. Lucas, A. Anadón, T. Oyake, K. Uchida, H. Adachi, J. Shiomi, P. A. Algarabel, L. Morellón, S. Maekawa, E. Saitoh, and M. R. Ibarra, Unconventional scaling and significant enhancement of the spin Seebeck effect in multilayers, Phys. Rev. B **92**, 220407(R) (2015).

[27] A. Anadón, R. Ramos, I. Lucas, P. A. Algarabel, L. Morellón, M. R. Ibarra, and M. H. Aguirre, Characteristic length scale of the magnon accumulation in Fe_3O_4/Pt bilayer structures by incoherent thermal excitation, Appl. Phys. Lett. **109**, 012404 (2016).

[28] R. Ramos, A. Anadón, I. Lucas, K. Uchida, P. A. Algarabel, L. Morellón, M. H. Aguirre, E. Saitoh, and M. R. Ibarra, Thermoelectric performance of spin Seebeck effect in Fe_3O_4/Pt-based thin film heterostructures, APL Mater. **4**, 104802 (2016).

[29] R. Ramos, T. Kikkawa, A. Anadón, I. Lucas, K. Uchida, P. A. Algarabel, L. Morellón, M. H. Aguirre, E. Saitoh, and M. R. Ibarra, Temperature dependence of the spin Seebeck effect in [Fe_3O_4/Pt](n) multilayers, AIP Adv. **7**, 055915 (2017).

[30] R. Ramos, I. Lucas, P. A. Algarabel, L. Morellón, K. Uchida, E. Saitoh, and M. R. Ibarra, Enhanced thermo-spin effects in iron-oxide/metal multilayers, J. Phys. D **51**, 224003 (2018).

[31] P. Jimenez-Cavero, I. Lucas, A. Anadón, R. Ramos, T. Niizeki, M. H. Aguirre, P. A. Algarabel, K. Uchida, M. R. Ibarra, E. Saitoh, and L. Morellón, Spin Seebeck effect in insulating epitaxial γ-Fe_2O_3 thin films, APL Mater. **5**, 026103 (2017).

[32] See Supplemental Material at http://link.aps.org/supplemental/10.1103/PhysRevB.108.035145 for the structures of the Me/Fe_3O_4 superlattices, DOS of Fe_3O_4, DOS of Me/Fe_3O_4 for Me=Au, Pt, Ir, Os, W, and Ta, and DOS of Me/γ-Fe_2O_3 for Me=Pt and Ta.

[33] P. Blaha, K. Schwarz, G. K. H. Madsen, D. Kvasnicka, and J. Luitz, *WIEN2k: An Augmented Plane Wave + Local Orbitals Program for Calculating Crystal Properties* (Technische Universität, Wien, 2014), www.wien2k.at.

[34] J. P. Perdew, K. Burke, and M. Ernzerhof, Generalized Gradient Approximation Made Simple, Phys. Rev. Lett. **77**, 3865 (1996).

[35] G. K. H. Madsen and P. Novák, Charge order in magnetite. An LDA+U study, Europhys. Lett. **69**, 777 (2005).

[36] P. Novák and J. Rusz, Exchange interactions in barium hexaferrite, Phys. Rev. B **71**, 184433 (2005).

[37] R. F. W. Bader, *Atoms in Molecules-A Quantum Theory* (Oxford University Press, Oxford, 1990).

[38] K. Knížek, M. Soroka, O. Kaman, J. Kuličková, P. Levinský, J. Hejtmánek, and Z. Jirák, Electronic and heat transport phenomena in the nanogranular thiospinel Fe_3S_4, Phys. Rev. B **103**, 245129 (2021).

[39] J. P. Wright, J. P. Attfield, and P. G. Radaelli, Charge ordered structure of magnetite Fe_3O_4 below the Verwey transition, Phys. Rev. B **66**, 214422 (2002).

[40] R. Grau-Crespo, A. Y. Al-Baitai, I. Saadoune, and N. H. De Leeuw, Vacancy ordering and electronic structure of γ-Fe_2O_3 (maghemite): a theoretical investigation, J. Phys.: Condens. Matter **22**, 255401 (2010).